FLOW PATTERN ANALYSIS OF AN OUTFLOW RADIAL TURBINE FOR TWIN-TURBINES-OWC WAVE ENERGY CONVERTERS

Laudino Rodríguez[a], Bruno Pereiras[b,*], Manuel García-Diaz[b], Jesús Fernández-Oro[b] and Francisco Castro[c]

[a] Centro Integrado de F.P. Mantenimiento y Servicios a la Producción de Langreo (C.I.F.P.M.S.P.)

Ciudad Tecnológica e Industrial Valnalón, Hornos Altos S/N, 33930, La Felguera, Spain

laudelinrg@gmail.com

[b] Department of Energy, University of Oviedo

Energy Building (EDZE), Campus de Viesques s/n, 33271, Gijón, Spain

* pereirasbruno@uniovi.es; garciadmanuel@uniovi.es: jesusfo@uniovi.es

[c] Department of Energetic and Fluidmechanics Engineering. University of Valladolid

Paseo del Cauce 59, 47011, Valladolid, Spain

castro@eii.uva.es

ABSTRACT

OutFlow Radial (OFR) Turbines have been recently proposed for Oscillating Water Column (OWC) devices based on a Twin Turbine Configuration (TTC). Previous experimental studies showed that these turbines are a feasible alternative to axial unidirectional turbines without rectifying systems.

In this paper, a validated CFD model is employed to achieve a better understanding on how the OFR turbine is working in an OWC energy converter for both direct and reverse modes. The turbine geometry corresponds to a second prototype proposed in a previous publication, with a total-to-static peak efficiency of 54%. The key of the performance in reverse mode is the vortical structure created within the blade-to-blade passage, almost choking the flow rate through the rotor. It is also concluded that increasing the outer blade angle leads to a worse performance in reverse mode, although the global performance is improved due to the rotor efficiency gain in direct mode. Finally, it has been also observed that the kinetic energy at the outlet during direct mode still remains as the major source of loss, penalizing the attainable maximum efficiency. Future work should be focused on the reduction of this residual energy to boost the application of these OFR turbines for TTCs.

KEY WORDS: Wave energy, OWC, Twin turbines, OutFlow Radial turbine, CFD

NOMENCLATURE

$A_R = \pi b D_m$	*Characteristic area*
b	*Blade span*
$C_A = 2\Delta P_{t-s}\, Q/\left(\rho(v_R^2+u_R^2)\pi b D_m v_R\right)$	*Input coefficient*
$C_T = 4T_o/\rho(v_R^2+u_R^2)\pi b D_m^2$	*Torque coefficient*
D_m	*Mean turbine diameter*
Q, q	*Flow rate*

Q_{max}	*Flow rate amplitude in unsteady conditions*
T_o	*Output mechanical torque*
T	*Period*
$uR = \omega D_m/2$	*Blade velocity at mean radius*
$v_R = Q/A_R$	*Reference radial velocity at mean radius*
u, v, w	*Velocity components (peripherical, absolute and relative)*
α, β	*Absolute and relative flow angles*
$\eta = T_o\ \omega / \Delta P\ Q$	*Steady Efficiency*
ΔP	Pressure difference
η_{vol}	*Volumetric efficiency*
$\bar{\eta}_{input}$	*Input mean efficiency*
$\bar{\eta}_{turbine}$	*Mean efficiency of twin-turbines set*
$\bar{\eta}_{system} = \bar{\eta}_{turbine}\ \bar{\eta}_{input}$	*Mean efficiency of the whole system*
ρ	*Air density*
$\phi = v_R/u_R$	*Flow coefficient*
Φ	*Flow coefficient in unsteady conditions*
ω	*Rotational speed*

Subscripts/superscripts

D / R	*Direct / Reverse*
t - s	Total-to-static
t - t	Total-to-total

1. INTRODUCTION

It is well known that ocean energy, despite being a great engineering challenge, it will be a hot spot among renewable energy resources. It is expected to steadily grow in the next years as one of the most promising renewable energy sources worldwide. It has been reported that several private companies have confirmed significant projects to be deployed in the next future [1,2]. In addition, the scientific community is promoting the use of these clean technologies through new investigations that shows their increasing applicability and functionality. Among Wave Energy converters, the Oscillating Water Column (OWC) concept appears as a top option because the most important parts of the device are placed out of the sea water, increasing the life expectancy and reducing maintenance. Detailed information and many references about the OWC concept can be found in [3].

Very first OWCs were equipped with unidirectional turbines in combination with a flow rectification system to take advantage of the bidirectional air flow in the chamber. However the use of these systems was soon discarded for being considered unpractical for large devices [3]. Therefore, the use of high-efficiency unidirectional turbines within OWC devices moved towards the introduction of bidirectional turbines to avoid the mechanical complexity of flow rectification system. A wide number of reports on bidirectional turbines is available in the open literature [3–5].

Nevertheless, the consideration of unidirectional turbines for OWC devices was never abandoned, and they have even gained popularity in recent times. The seed of this renewed interest on unidirectional turbines is probably based on several considerations such as new manufacturing technologies, new operational procedures, new control systems, etc. However, in the authors' opinion, the presentation of the Twin Turbines Configuration (TTC) in [6] has probably played a major role on the reborn of unidirectional turbines for OWC devices. The key of this system is that the malfunction of an unidirectional turbine when working in reversed flow, makes the turbine itself to act as a backflow preventer, thus avoiding the need of any flow rectification system. Therefore, the TTC is based on the use of two turbines, one of them working normally (direct mode) while the other is working as a backflow preventer (reverse mode). A sketch of this system is shown in Figure 1. Basically, the air from the chamber is pushed towards the atmosphere (namely exhalation), so the flow generated by the OWC goes through the turbines. One of the turbines is working in direct mode (producing energy), whereas the other one is working in reverse mode (not producing energy). Following, due to the oscillating movement of the waves, when the exhalation process is over, the inhalation starts and the air is aspirated from the atmosphere to the chamber with the turbines switching their roles. Note that the flow rate distribution between the turbines, which are working under the same pressure difference (chamber-ambient), is determined by the performance curve of both turbines, which differs depending on the working mode.

The pioneering work made by V. Jayashankar [6], based on unidirectional axial impulse turbines previously published [7], showed that a remarkable efficiency could be reached in a TTC, thus encouraging for further investigations. Following works such as [8–11] analysed TTC based on a pair of axial impulse turbines, revealing in that these turbines have a poor performance as a backflow preventer, compromising the efficiency of the whole system [11]. In order to overcome this problem, OutFlow Radial (OFR) turbines were suggested as a solution [12,13], since these kind of turbines can reach non-steady efficiencies comparable to those achieved by axial turbines.

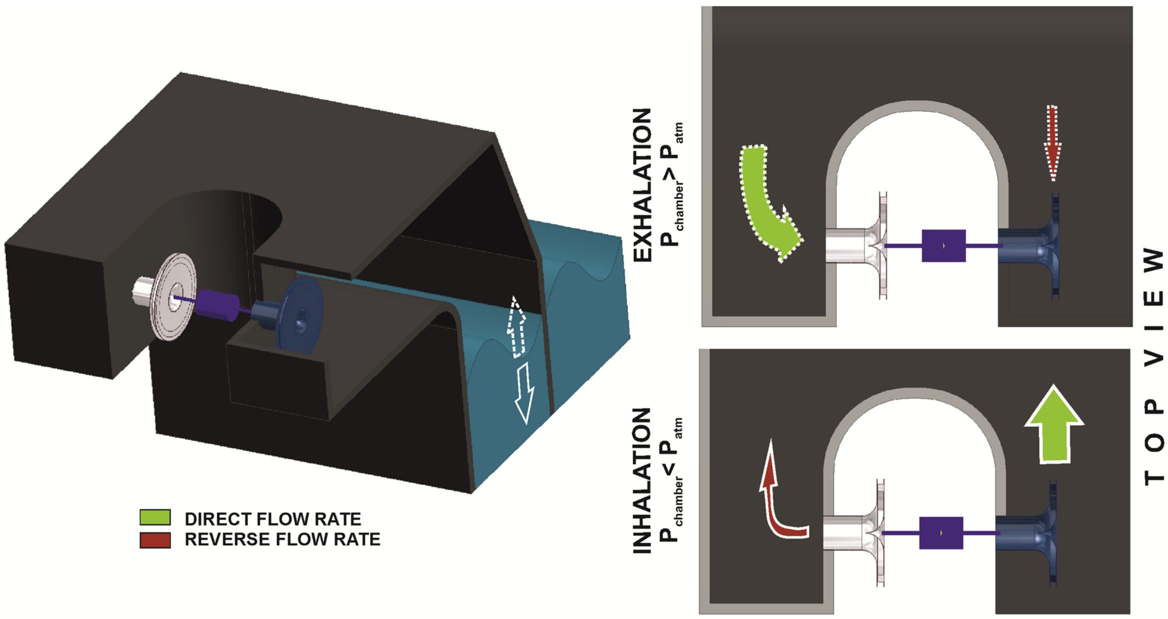

Figure 1. OWC equipped with twin radial turbines.

Recently, the performance of non-axial unidirectional turbines has also been studied to work as the Power Take-Off (PTO) element within other configurations of OWC devices. In particular, two new patents conceived by the IST Wave Energy Group have appeared in 2018 [14,15]. The first one is equipped with a rotor composed of two InFlow Radial (IFR) turbines in combination with guide vanes and a check valve, whereas the second one shows a system to be equipped with two turbines, either IFR or axial impulse turbines, in combination with a rectification system. It has been reported that, neglecting the loss at the diffuser, a peak efficiency of 74% can be reached in steady performance for the first design [16].

In parallel, another configuration has been recently patented by Wave Swell Energy Limited [17] already showing some promising results with its new system [18]. This configuration is a different concept of the OWC since it produces energy only when the free surface within the chamber is descending. With such constraint, it is clear that an unidirectional turbine is obviously the ideal selection for such device. The design process of a IFR turbine to be installed in this device can be seen in [19,20].

All these recent works consider the use of radial turbines as the best option for new designs of OWC devices. Moreover, speaking about bidirectional turbines and depending on the OWC location, a radial turbine could be the best choice due to its larger damping [21]. Therefore, considering all this lately research, the position of radial turbines as PTO for OWCs has been significantly strengthened.

In this paper, the work presented by the authors is focused on the development of a TTC equipped with two OFR turbines, as shown in Figure 1, right. It is a similar design to that presented in [15] but with no flow rectification system, which clearly differentiates this new proposal. Therefore, the performance of the turbine to choke the flow in reverse mode has been treated carefully because this is completely critical to guarantee the viability of the design. Otherwise, like previously observed in [11], up to one third of the flow generated by the OWC can be wasted through the turbine that is supposed to be working as a backflow preventer. Precisely, the authors have demonstrated that the use of OFR turbines reduces that air leakage tremendously, with a blockage effectiveness over 90% [13] . On the other hand, it is also prescribed that the efficiency in direct mode must be improved so the non-steady efficiency could be increased over 40% for sinusoidal flow conditions.

The performance of the OFR turbine presented in [13] is now analysed using CFD techniques to describe the flow field and envisage geometrical modifications for further optimization. Special attention has been devoted to study the effect of changing certain geometrical parameters like the outflow angle, the blade chord or the number of blades. The obtained results have been compared to those obtained by the first prototype [12]. The numerical model developed, its validation through comparison with experimental data and the detailed discussion of the results are the main contributions of the present paper.

2. MATERIALS AND METHODS

2.1. GEOMETRY

The geometry of the OFR turbine analysed in this paper is taken from a previous work [13], being composed of a single rotor with 2-D blade profiles. Neither downstream nor upstream guide vanes have been considered for this turbine. Figure 2 shows the general shape of the blade profile, defining the basic geometrical parameters. The main dimensions of both optimized and first prototype blades are given in Table 1.

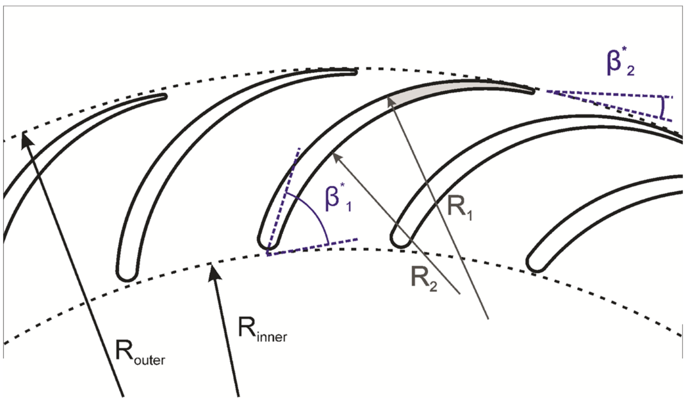

Figure 2. Main view and dimensions of the blade profile for the OFR turbine.

Table 1. Main dimensions [mm] of the optimized and first prototype blades

	Chord [mm]	*R1 ; R2* [mm]	*Rinner* [mm]	*Router* [mm]	*β1* [º]	*β2* [º]	*Blade number*
Optimized Prototype	*43.2*	*28.8 ; 28.8*	*75*	*100*	*65*	*11*	*24*
First Prototype	*50.4*	*28 ; 29*	*75*	*99.2*	*65*	*5*	*30*

2.2. NUMERICAL MODEL

The ANSYS Fluent Solver v16 was used to solve the incompressible (U)RANS set of equations over one single rotor passage of the turbine because of the circumferential periodicity of the domain. This is a common solution used for CFD models to save computational resources, and it is typically implemented following the sidewalls parallel to the centerlines of blades and vanes. However, This usually leads to highly-twisted domains which are difficult to mesh when orthogonal or hexaedrical grids are desired. In this case, a special feature concerning the periodic boundaries of the numerical domain has been adopted to improve que mesh quality (see Figure 3, left), thus introducing straight periodic surfaces in the radial direction. Although this results in rotor blades that are cut in the mid-passage, the numerical results (which are shown later) were found to be accurate to validate this strategy.

The mesh and the boundary conditions implemented are shown in Figure 3. The mesh has been built using the grid modeller GAMBITv2.4.6 over an angular sector comprising 15 deg (1/24 of the full annulus). A total number of 740K cells has been employed for the whole domain, which was divided in three separated blocks: 1) the rotor volume which is non-regular mesh composed of hexaedrical cells with boundary layer mesh on the blades; 2) and 3) inner and outer domains respectively, both are completely mapped mesh with structured cartesian cells. The resulting mesh is of a mid-high quality with a maximum skewness of 0.77 (Gambit criteria) and the 80% of the mesh below 0.4.

For convenience, two set of interfaces have been introduced in the computational domain. This allowed the use of non-conformal grids between the different blocks of the geometry and the relative displacement of the blades with the sliding mesh technique. Note that, despite not being necessary due to the absence of guide vanes, the Moving Mesh approach was used because this single rotor geometry was simulated in batch within other geometries equipped with guide vanes.

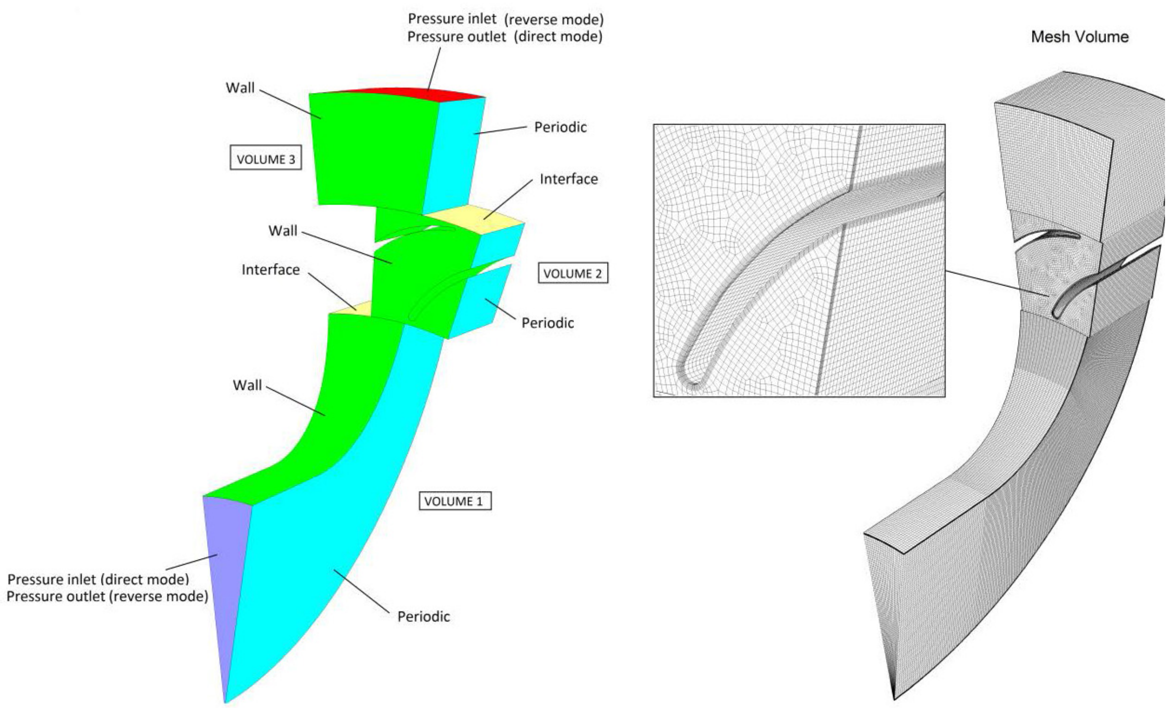

Figure 3. Left: Computational domain and boundary conditions. Right: Mesh details.

For the turbulent closure, the realizable k-ε turbulence model, already validated in previous works on radial turbines [12,22], has been used for the bulk of simulations. In addition, an Enhanced Wall treatment was also adopted, employing special care on the walls to obtain y+ values in the correct range. The time-dependent term was discretized with a second-order implicit scheme. The pressure-velocity coupling was recreated through the SIMPLE algorithm. The high-order Monotone Upwind Scheme for Conservation Laws (MUSCL) has been used for the discretization of the convection terms and the classical central difference approximation was considered for the diffusion terms.

The time step was set to 10^{-4} s, resulting in 40 time steps per blade passing period. The residuals were set to 10^{-4} and the convergence was met after approximately 30 iterations per time step for all the resolved equations. Four full-annulus rotations of the periodical domain were simulated to reach global convergence, with approximately 4 hours of CPU time per case simulated. The simulations were performed in a 4-units cluster of the following characteristics: intel i5 2.67GHz, 2x2 GB RAM.

The simulations were performed considering that the turbine rotates unsteadily but under quasi-steady flow conditions. This assumption is perfectly justified through the reduced frequency of the turbine (the ratio between the blade passing period and the period of the wave cycle) which turns to be of order 10^3. This allows to maintain constant the boundary conditions (flow rate and rotational speed) in each simulation. Finally, the performance of the turbine for other thorough-flow conditions is obtained by adjusting the inlet boundary conditions.

2.3. DATA POST-PROCESSING

The performance curve of the turbine is given in terms of the usual non-dimensional coefficients used for OWC applications.. The torque, input and flow coefficients (C_T , C_A , ϕ) as well as the total-to-static efficiency (η) are defined as:

$$C_T = \frac{4 \cdot T_o}{\rho \cdot (v_R^2 + u_R^2) \cdot \pi \cdot b \cdot D_m^2} \qquad C_A = \frac{2 \cdot \Delta P_{t-s}\, Q}{\rho \cdot (v_R^2 + u_R^2) \cdot \pi \cdot b \cdot D_m \cdot v_R} \qquad \phi = \frac{v_R}{u_R} \qquad \eta = \frac{C_T}{C_A \cdot \phi} \qquad Eq.\ 1$$

where ρ is the air density, T_o is the mechanical torque, $\Delta P_{t\text{-}s}$ is the total to static pressure drop, Q is the flow rate, D_m is the rotor diameter ad midspan, b is the blade span, A_R is the cross-flow area at the midspan radius ($D_m/2$), v_R is the reference velocity and u_R is the blade speed at $D_m/2$. Note that, the efficiency, which is the ratio of shaft power output to pneumatic power input, can be expressed in terms of the previous non-dimensional coefficients.

In order to extend the analysis, the CFD results obtained from the steady flow conditions for the turbine performance are employed as input data for a further analytical study under non-steady flow conditions. This methodology, widespread in the bibliography [9,11,23], is based on the assumption of the quasi-steadiness of the flow through a OWC turbine with respect to the wave motion time-scale, which is typically modelled with a sinusoidal response according to:

$$Q_{Total} = Q_{max} \cdot sin\left(\frac{2\pi t}{T}\right) \qquad Eq.\ 2$$

Where Q_{max} is the maximum flow rate generated by the OWC within a wave cycle, T *is* the period of the wave (typically a few seconds) and t is the current time.

During operation, both turbines of the twin system are exposed to the same pressure difference. However, their performance is switched from direct to reverse mode and vice versa according to the sign of the pressure difference. Hence, the total outgoing flow rate transferred from/towards the chamber is the combination of both direct (Q_D) and reverse (Q_R) mode flow rates:

$$Q_{Total} = Q_D + Q_R \qquad Eq.\ 3$$

Consequently, the volumetric efficiency of the OWC device can be determined as the ratio between those direct and the total flow rates, according to:

$$\eta_V = \frac{Q_D}{Q_{Total}} = \frac{Q_D}{Q_D + Q_R} \qquad Eq.\ 4$$

On the other hand, the turbine efficiency is also relevant, so it must be evaluated in combination with the efficiency of the twin system. Precisely, this can be assessed, splitting the OWC efficiency in two terms, according to the following expression:

$$\bar{\eta}_{system} = \frac{\frac{1}{T}\int_0^T \omega \cdot T_o \cdot dt}{\frac{1}{T}\int_0^T \Delta P_{t-s} \cdot Q_{Total} \cdot dt} = \underbrace{\frac{\frac{1}{T}\int_0^T \Delta P_{t-s} \cdot Q_D \cdot dt}{\frac{1}{T}\int_0^T \Delta P_{t-s} \cdot Q_{Total} \cdot dt}}_{\bar{\eta}_{input}} \cdot \underbrace{\frac{\frac{1}{T}\int_0^T \omega \cdot (T_{oD} + T_{oR}) \cdot dt}{\frac{1}{T}\int_0^T \Delta P_{t-s} \cdot Q_D \cdot dt}}_{\bar{\eta}_{turbine}} \qquad Eq.\ 5$$

Or more compactly:

$$\bar{\eta}_{system} = \bar{\eta}_{input} \cdot \bar{\eta}_{turbine} \qquad Eq.\ 6$$

The so-called input efficiency, $\bar{\eta}_{input}$ is related to the volumetric efficiency (η_{vol}) of the OWC chamber, but in terms of power instead of flow rates only. Additionally, the turbine efficiency, $\bar{\eta}_{turbine}$ is the net efficiency of the twin turbines, considering the resistant torque (T_{oR}) produced in the reverse mode. In this case, the torques must be introduced within the calculation taking into account their sign.

Alternatively, the system flow coefficient is also defined as the ratio between the bulk velocity through both turbines, considering the total flow rate, and the reference tangential velocity, i.e.:

$$\Phi_T = \frac{Q_{Total}}{\pi \cdot D_m \cdot b \cdot u_R} \qquad Eq.\ 7$$

Apart from the main dimensionless coefficients, a closer look to the flow pattern in the different elements of the turbine will be also presented. In particular, the local pressure drop through the different sections A, B, C and D (see Figure 4) will be discussed in detail to characterize the internal losses of the turbine. Additionally, the kinetic energy at the outlet will be also quantified for different flow conditions as another significant source of loss.

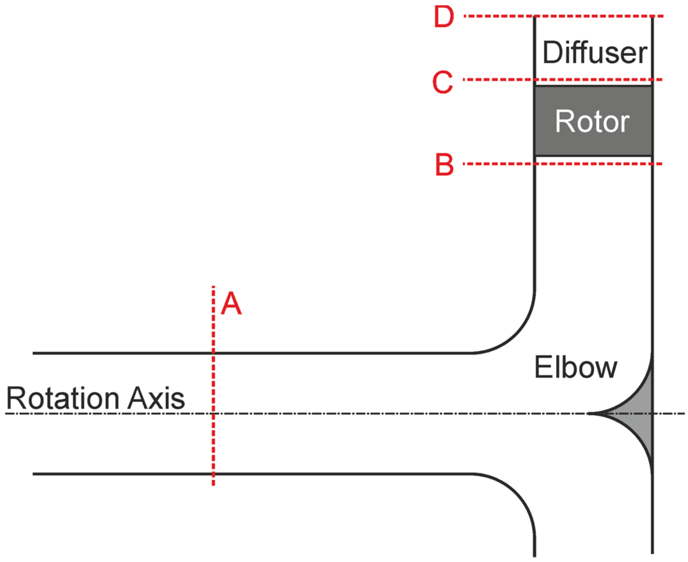

Figure 4. Streamwise sections for the analysis of the loss distribution in the turbine.

To conclude this section, the reference criteria adopted for the discussion of the blade angles in following sections is now shown in Figure 5. Note that the angles are always measured counter-clockwise for both performance modes, direct and reverse. The zero reference is different between the modes in order to obtain angles below 180 degrees.

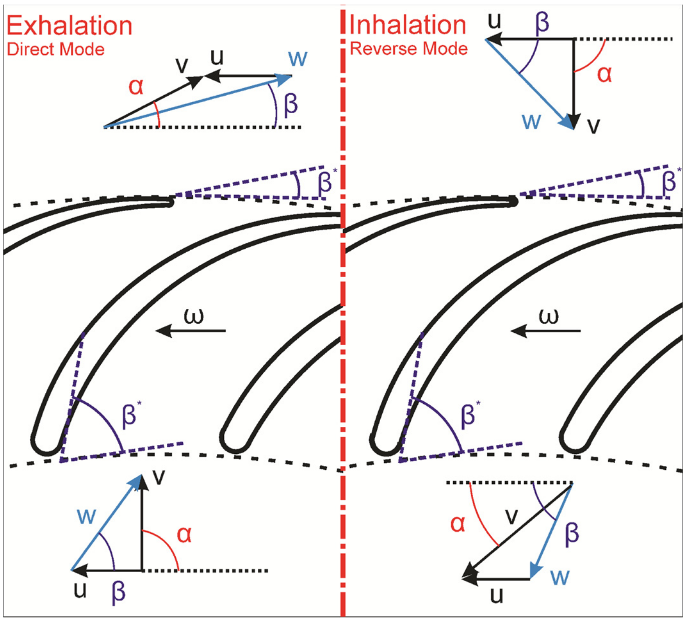

Figure 5. Reference angles and velocity relationships for both direct and reverse modes.

3. CFD VALIDATION, RESULTS AND DISCUSSION

3.1. VALIDATION

For validation purposes, the CFD results of the model are compared to the experimental results for the same geometry (extracted from [13]) in Figure 6. All the non-dimensional coefficients reveal the close agreement achieved by the numerical model to reproduce the performance of the turbine in both modes, direct and reverse, which corresponds to positive and negative flow coefficients respectively. The agreement in case of the input coefficient (C_A) (Figure 6, top) presents higher differences, with maximum deviations of 10 and 16% in the direct and reverse modes respectively, but without compromising the overall trends that are perfectly reproduced. The agreement in case of the torque coefficient (C_T) (Figure 6, middle) is particularly good, with maximum discrepancies always below 6% in direct mode. In the reverse mode relative differences up to 15% are reached for the smaller flow coefficients. The comparison in terms of steady total-to-static efficiency (Figure 6, bottom) is also remarkable, showing differences always below 5%.

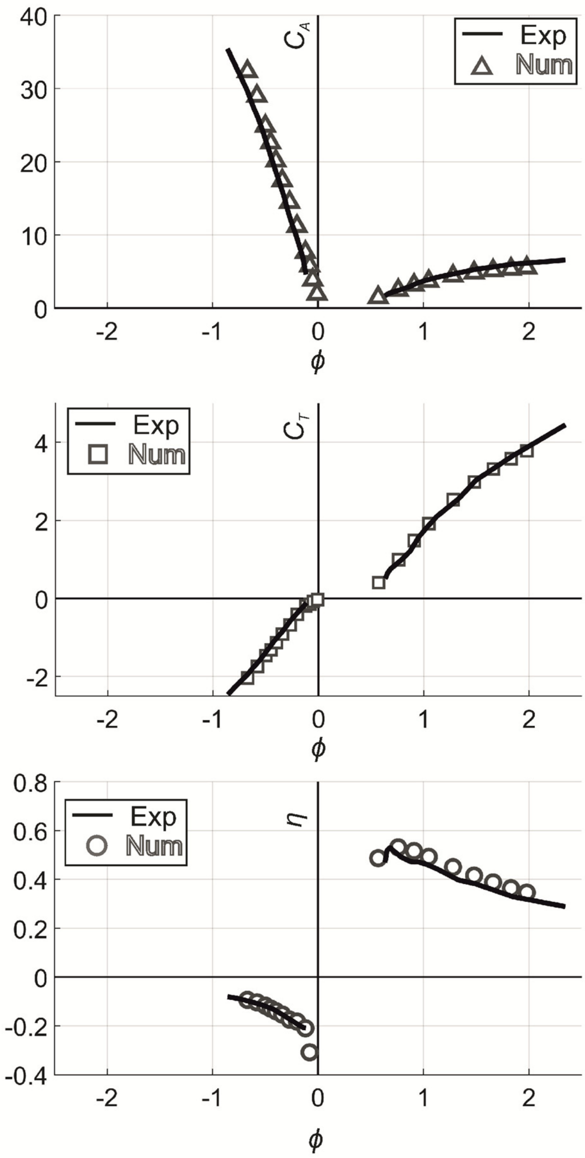

Figure 6. Comparison between the CFD results and the experimental tests from [13].

The comparison concludes the reliability of the CFD model to predict the performance of the turbine. It also reveals that the employment of radially-straight sidewalls as boundary conditions allowed to reduce the complexity of meshing operations with no penalty on the accuracy of the results. This validation also encourages to go further in the analysis of the flow patterns computed by the model, even promoting its use for the optimization of some parts of the turbine.

From now on, and to avoid confusion with the explanations, only CFD results will be presented in the following sections. In particular, these will concern the comparison between computational results of the first prototype [12] and the optimized one [13].

3.2. GENERAL PERFORMANCE

As a starting point, the numerical curves of both first and optimized geometries are compared in Figure 7. It is noticeable that the total-to-static efficiency of the optimized geometry is superior by 8-9% in direct mode with respect to the first design (Figure 7, bottom). This improvement is not associated to a larger torque, as expected from the lower flow deflection made by the optimized rotor (simple kinematics considerations within the momentum equation would confirm that - see Table 1). In fact, the optimized rotor provides even less torque than the first prototype (Figure 7, middle). The explanation is given by the significant loss reduction in the optimized rotor when is working in direct mode, which leads to that remarkable efficiency increase. On the other hand, it is well reported that the performance when working as a backflow preventer (negative flow coefficients) is critical. With respect to the input coefficient C_A (Figure 7, top), a similar performance is found for both turbines in the reverse mode, but with larger values in case of the first prototype when works in direct mode. This implies that, under the same pressure difference, one TTC equipped with the optimized geometry would have a larger flow rate running through the turbine working in direct mode, thus implying a larger total efficiency of the system under non-steady conditions will be higher.

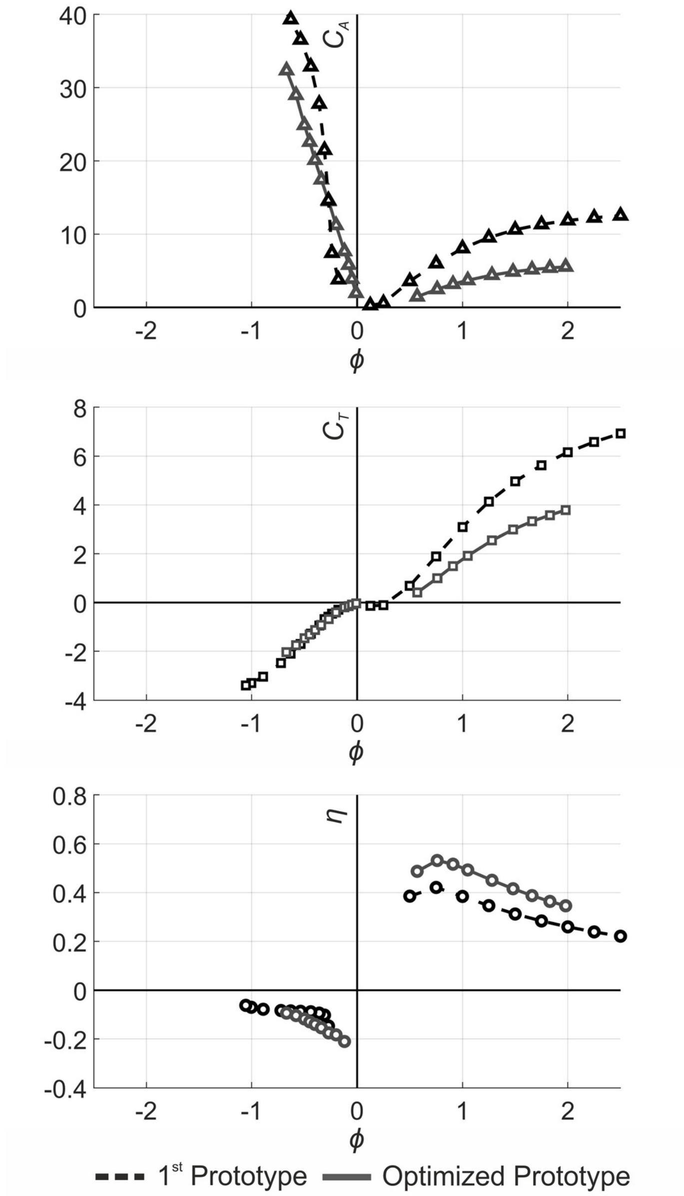

Figure 7. Performance comparison of CFD results between the first prototype, from [12], and the optimized one (present study).

Additional results corresponding to the turbine performance under non-steady conditions are shown in Figure 8. The plot, which compares the volumetric efficiency (see eq. 4) presented by both prototypes, gives a clear idea about the blockage achieved during the reverse mode. The optimized geometry reaches values above 90% whereas the maximum value for the first prototype never exceeds the

78%. Note that this feature, in combination with the efficiency rise gained in the direct mode, contributes to an impressive global improvement of the optimized turbine. This is also shown in Figure 9 (bottom), where the maximum system efficiency rises above 11% with respect to the original prototype. This improvement in the non-steady efficiency of the system ($\bar{\eta}_{system}$) is sustained in both input and turbine non-steady efficiencies ($\bar{\eta}_{input}$ and $\bar{\eta}_{turbine}$ in Figure 9, top and middle, respectively).

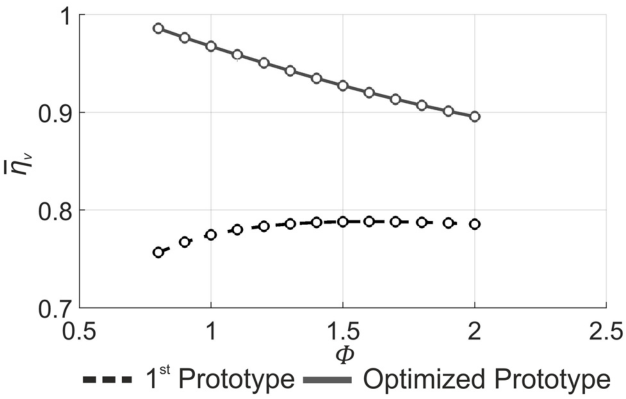

Figure 8. Volumetric efficiency of both prototypes under sinusoidal flow conditions.

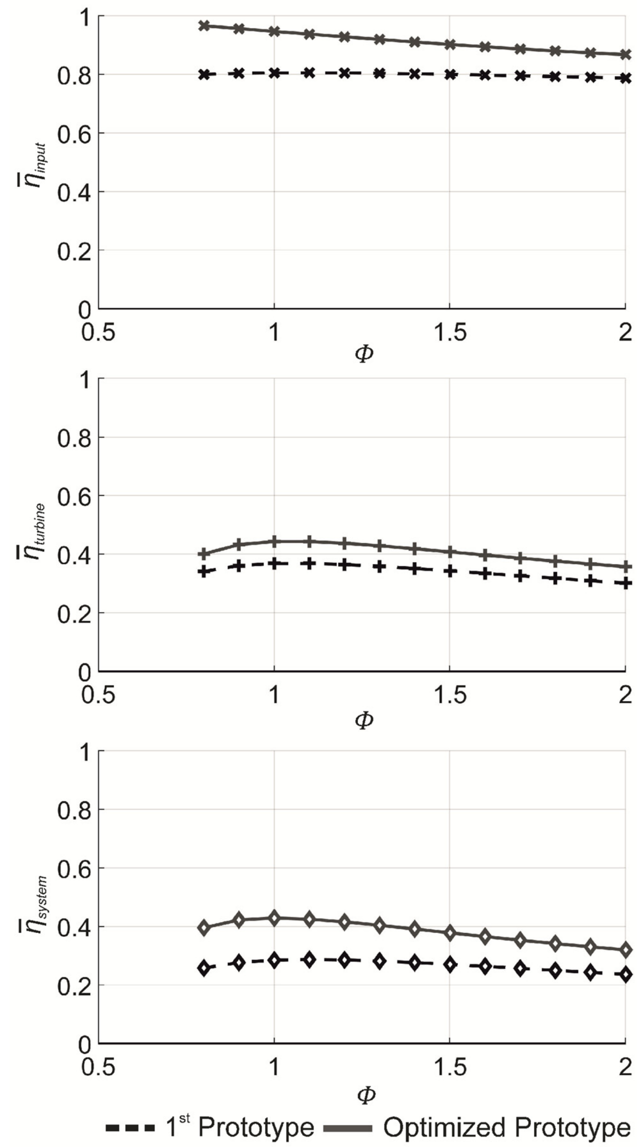

Figure 9. Non-steady efficiency of the system for both prototypes under sinusoidal flow conditions.

Following, the numerical flow fields obtained from the CFD model will be analysed in detail to provide further physical insight over the improvement gained with the optimized turbine. In addition, this analysis will help to identify other possible design limitations and propose new geometrical modifications.

3.3. ANALISIS OF THE FLOW PATTERN IN DIRECT MODE

Note that, as reported in [13], the changes made on the optimized geometry were positive concerning two points of view: 1) Improvements in direct mode were achieved mainly by the reduction of the residual kinetic energy at the outlet and, 2) better performance as a backflow preventer was obtained due to the lower losses in direct mode whereas the performance in reverse mode remains similar. However, the following CFD results have provided more insight, revealing that the impact of these modifications is broader, showing additional unexpected features..

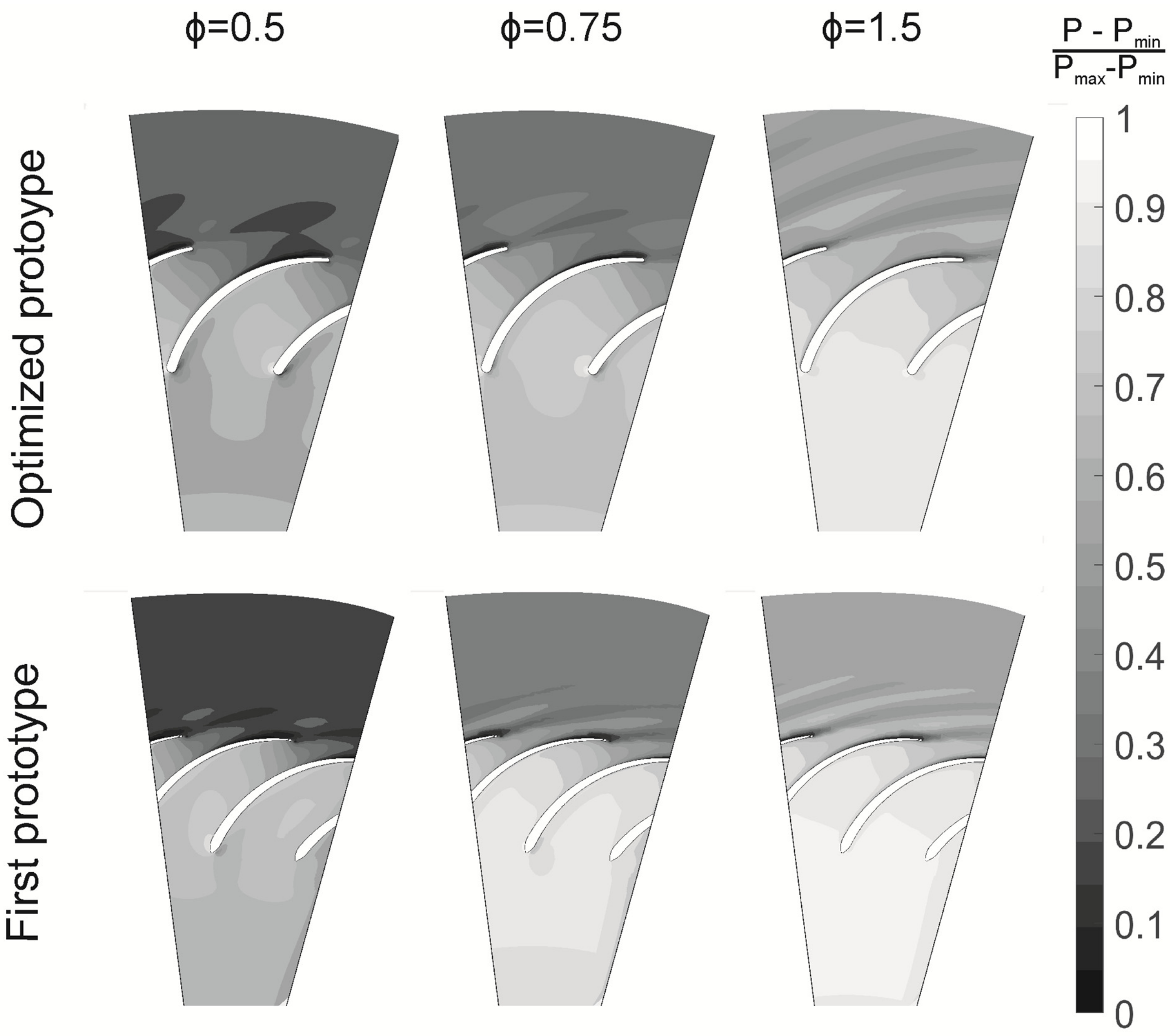

Figure 10. Contours of normalized total pressure for both optimized (top) and first (bottom) prototypes in direct mode.

Figure 10 shows the contours of normalized total pressure for both geometries in direct mode. Low (ϕ = 0.5), nominal (ϕ =0.75) and high (ϕ =1.5) flow rate coefficients are represented in the blade-to-blade plane of the rotor at midspan. Both prototypes present a similar flow pattern, characterized by (1) an almost negligible flow detachment at the rotor leading edge, (2) unnoticeable difference in the flow separation at the suction side and (3) wakes gaining importance as the flow coefficient increases. However, the effects of the new blade profile are also significant, mainly observed as (1) weaker pressure gradient at the rotor outlet (compared to the first prototype) and (2) a lower intensity of the wakes, associated to less tangential component of the flow velocity at the rotor outlet (see wake orientation). Note that most of these differences are gathered close to the rotor discharge, indicating that the rotor performance is strongly affected by the outlet geometrical parameters. Precisely, Figure 11 demonstrates that after increasing the rotor external angle from 5 to 11 deg (Table 1), the total-to-total rotor efficiency is significantly increased (up to 15%), also implying a valuable reduction of the residual kinetic energy at the outlet. Although this fact may basically explain the improvement of the total-to-static efficiency of the optimized prototype (Figure 7, bottom), a deeper analysis is required to take into account the change in the rotor solidity.

The impact of increasing the external angle on the geometry is associated to a lower curvature on the blades and a wider cross-section at the outlet, that leads to a lesser flow deflection. In addition, less turbulence is generated within the blade passages and the intensity of the wakes is also reduced. Alternatively, the position of the best efficiency point of the rotor, which is placed around $\phi \approx 1$ for both geometries, is determined by the inner blade angle (corresponding to the leading edge during direct mode). Figure 12 compares the flow angles (β) with respect to the blade angles (β*) in both geometries, revealing that they matched when the flow coefficient is $\phi \approx 1.5$. This is consistent with the bibliography where it is well reported that the optimum incidence angle does not correspond to the perfect matching. Typically, small incidence angles use to lead to a better performance of the blades [24]. However, radial outflow turbines are relatively insensitive to the incidence angle within the range of [-20,10] degrees with respect to the perfect matching [25]. Effectively, this is confirmed for the present OFR turbine where the total-to-total rotor efficiency (Figure 11) is maintained close to the maximum for that range of incidence angles. Moreover, the flow deviation at the rotor outlet with respect to the trailing edge angle is independent of the incidence angle, as reported in [25,26] for outflow turbines. Figure 12 shows that the flow deviation is around 10 degrees for both geometries at any flow coefficient, being completely independant of the incidence angle.

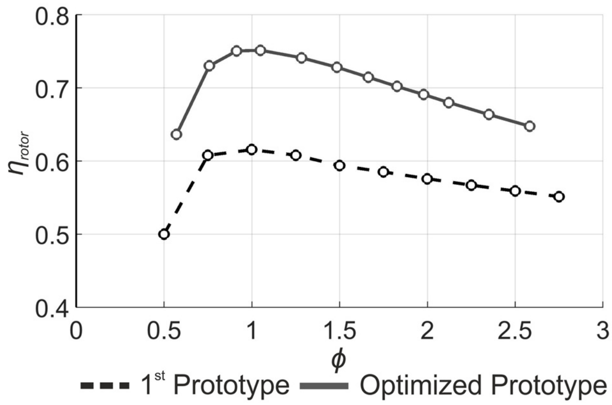

Figure 11. Comparison of the total-to-total efficiencies of first and optimized rotors.

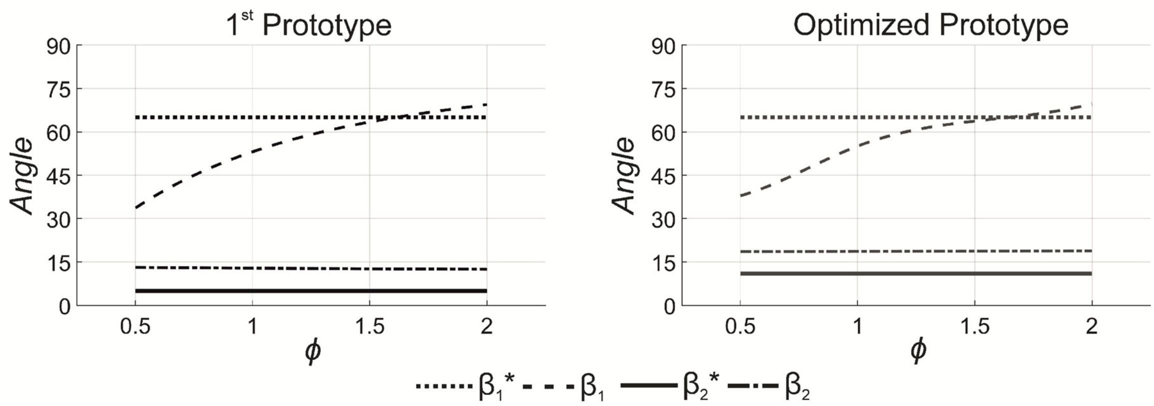

Figure 12. Comparison of flow angles (β_1 , inlet and β_2 outlet) and blade angles (β_1^*, LE and β_2^*, TE) in direct mode for the first prototype (Left) and the optimized turbine (right).

On the other hand, the modification of the rotor solidity results in two opposite effects over the turbine in direct mode: (1) as expected, a higher solidity improves the flow guidance. This is shown in Figure 13, where the relative flow deviation is plotted against the flow coefficient for different solidity values. Large solidities also increase the output torque, with a flow deviation which is slightly dependant on the flow incidence. Alternatively, solidities below 1.08, which corresponds to 18 blades, are not recommended because the guidance is severely penalized, plunging the turbine efficiency off. (2) Higher solidity values also leads to a smaller cross-section of the blade passage, generating larger velocities with major losses and wake deficits. Hence, the residual kinetic energy at the turbine outlet will be larger as well, mainly associated to a higher tangential velocity.

In summary, the optimum solidity in direct mode has been found for 20 blades as it can be deduced from Figure 14, where maximum steady efficiencies for both rotor only and complete optimized turbine are represented for different blade numbers (i.e. against the solidity). Anyway the solidity also plays a major role in the performance of the reverse mode. In particular, the performance as a backflow preventer improves if the solidity increases, but the performance in direct mode gets worse as the solidity is progressively increased with respect to the optimum value. As an intermediate solution, a turbine equipped with 24 blades provides a well-balanced behaviour, as it was reported in [13].

Obviously, the changes made on the rotor geometry, turning the external angle from 5 to 11 deg and the solidity from 30 to 24 blades, affect the performance of the downstream components. Figure 15 shows the relative loss distributions across the turbine for both prototypes, according to the parts presented in Figure 4. Note that two considerations are relevant here: (1) the loss of the first prototype is larger in absolute values, see Figure 7, and 2) the results are plot for each element in terms of percentage of loss with respect to the total loss, where the power generated by the rotor has been excluded and the kinetic energy at the outlets have been considered also as a loss.

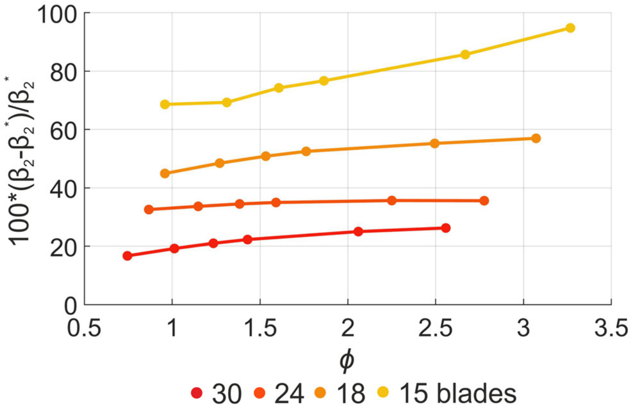

Figure 13. Percentage of flow angle deviation with respect to the external blade angle.

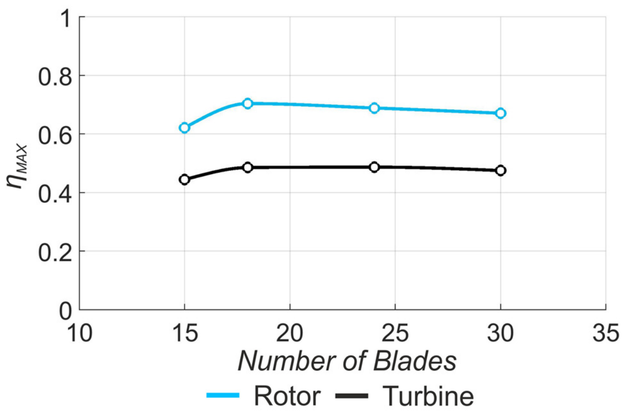

Figure 14. Rotor and turbine maximum steady efficiencies in direct mode as a function of the number of blades (i.e. solidity).

The distribution of losses in Figure 15 reveals that the loss within the rotor has been reduced by 4-10% in the optimized turbine depending on the flow coefficient, being this reduction more important for higher flow rate coefficients. In addition, it is observed that the most relevant source of loss in both turbines is the outlet kinetic energy, despite the reductions introduced in the blade external angle to minimize the outlet tangential velocity. At higher flow rates, this component is larger in the optimized geometry (68% against 59% in the original prototype at $\phi = 2$). However, in absolute terms, the value of the kinetic energy loss had been reduced with respect to the levels of the first turbine. Whatever the case, this high kinetic energy at the outlet, specially manifested as an important tangential velocity, is significant at flow coefficients over the best efficiency point, and envisages the opportunity for introducing a counter-rotating rotor at the outlet to take advantage of this residual energy.

It is also interesting to see how a downscaling of the outlet velocity in the rotor in the case of the optimized geometry has led to a notable reduction of the losses in the diffuser in the direct mode. Moreover, the connection elbow, with the same geometry for both prototypes, has increased its relative importance because of the loss reduction in the rest of the elements.

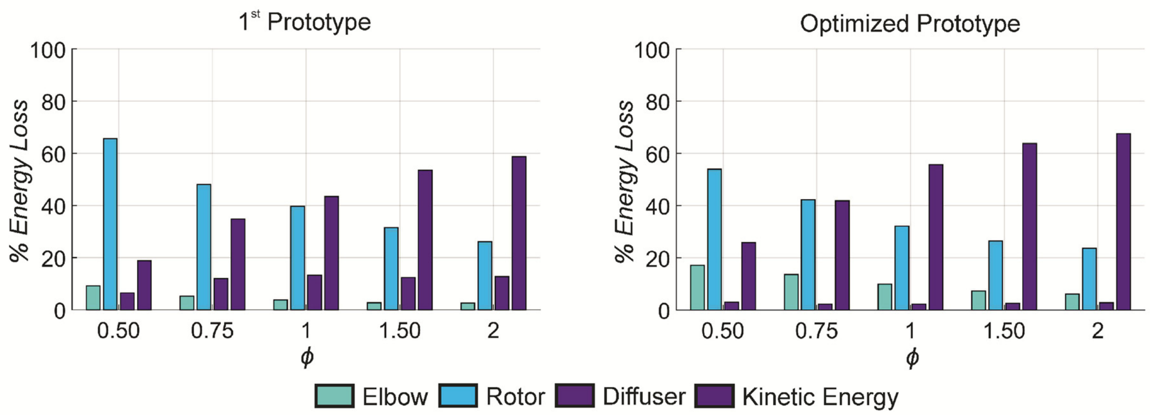

Figure 15. Comparison of the loss distribution in direct mode between the different elements of the first (left) and the optimized prototype (right).

3.4. ANALYSIS OF THE FLOW PATTERN IN REVERSE MODE

Figure 7 concluded that the total loss are slightly lower for the optimized prototype in reverse mode. Hence, it is expected that the flow patterns and the loss distribution in both geometries will present very similar characteristics in a closer look to the turbine performance. Figure 16 represents the normalized total pressure in the blade-to-blade plane for both geometries and two different flow coefficients. The contour maps reveal two clear regions within the blade passage, separated by a strong pressure gradient, which do not depend on the geometry or the flow coefficient. The first one is a low-velocity recirculation zone in the vicinity of the pressure side of the blades, while the second one a high-speed jet close to the suction side of the blades. Those regions are plainly discerned in Figure 17, where the pathlines through the rotor have been plotted for the optimized geometry at $\phi \approx -0.45$. Figure 17 also shows that the stagnation point is not placed at the blade leading edge in reverse mode (the external edge of the blade). On the contrary, it has been displaced at the suction side towards the 70% of the chord approximately. From the stagnation point, the flow is diverted with one portion going inwards through the rotor passage, while the other moves outwards creating a strong swirl at the rotor inlet (external part in reverse mode) that chokes most of the rotor inlet. Therefore, the flow crossing the rotor is forced to pass through a narrow path, creating a high velocity jet within the rotor passage and a secondary vortex at the inner part of the rotor channel. All these phenomena explain why the blockage in reverse mode is so good for these OFR turbines, reaching values of the volumetric efficiency over 90% as previously reported in Figure 8.

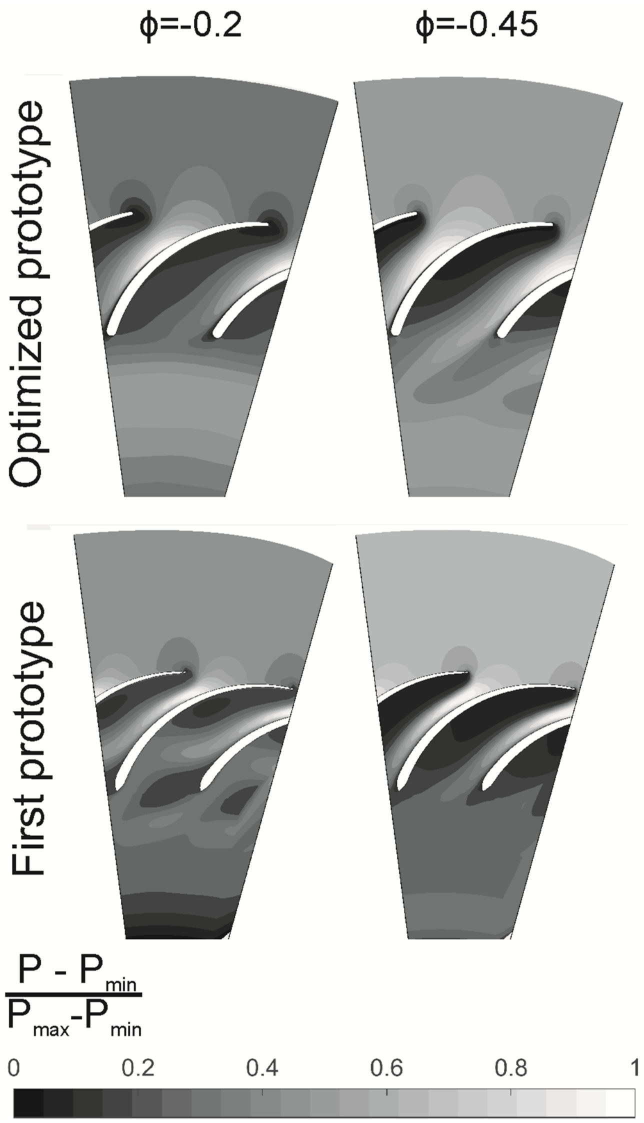

Figure 16. Contours of normalized total pressure in reverse mode for both optimized (top) and first (bottom) prototypes.

Figure 16 also illustrates some relevant differences in the flow patterns of both prototypes. The trail followed by the reverse flow within the rotor passage is even narrower in the first prototype as suggested in the contour maps of the figure. This is particularly clear in the case of the higher flow coefficient of the reverse mode ($\phi \approx -0.45$) and explains why the rotor of the first prototype shows a better performance as a backflow preventer at higher flow coefficients (advanced in Figure 7). To quantify the differences, Figure 18 compares the pressure drop coefficient in the rotor (made non-dimensional with the blade kinetic energy) as a function of the flow coefficient. It is observed that the blockage is similar for all the flow coefficients (slightly increased for higher ones), being almost four times more intense in the case of the first prototype than in the optimized one (almost four times higher).

Finally, Figure 16 also reveals flow separation in the trailing edge of the blades in the case of the first prototype. This is responsible for the progressive rise of the dimensionless loss reported in Figure 18 for smaller flow coefficient ($\phi \approx -0.2$).

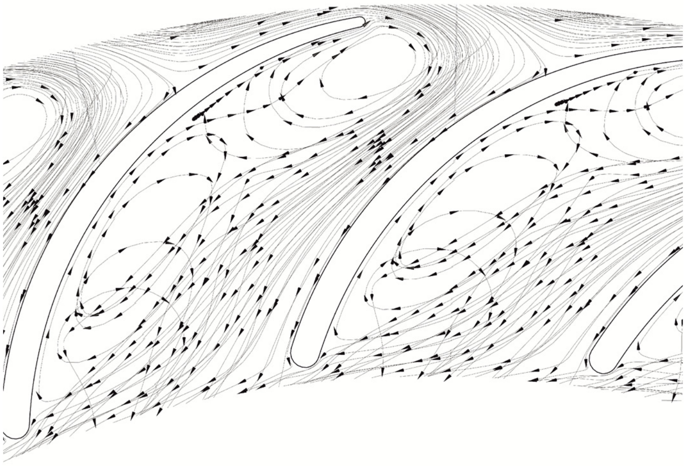

Figure 17. Pathlines in reverse mode within the rotor passages of the optimized geometry at flow coefficient ϕ=-0.45.

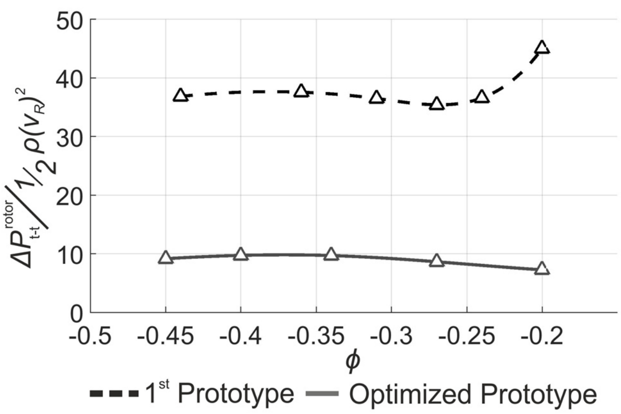

Figure 18. Dimensionless pressure difference across the rotor for both geometries in reverse mode.

To conclude this section, the loss distribution across the turbines is also analysed in the reverse mode (Figure 19). A first look to the results highlights the major role played by the elbow where a strong swirl is created due to the tangential flow velocity that leaves the rotor during the reverse mode. Since the flow pattern at the rotor outlet in reverse mode shows some differences between both prototypes, the intensity of the swirl created at the elbow differs as well. Actually, this was already pointed out as a critical source of loss for IFR turbines [12,22], even more critical than the rotor itself.

In fact, he most noticeable result is that, the importance of the loss generated in the elbow for the optimized geometry (significantly larger than in the first prototype). This is clearly related to the power dissipated by the rotor, which is relatively more important in the first prototype, reducing the contribution of the loss at the elbow (already discussed in Figure 18). The loss intensity, associated to the highly- narrowed section presented by the rotor of the first prototype, is definitive to understand these distributions. This explains that the real difference between both geometries for the reverse mode is due to the geometrical changes in the rotor profile, related to the external blade angle. Another typical feature of the reverse mode, as shown in Figure 19, is that the contribution of the kinetic energy loss at the outlet is practically equal in both prototypes, with a completely negligible loss in the diffuser.

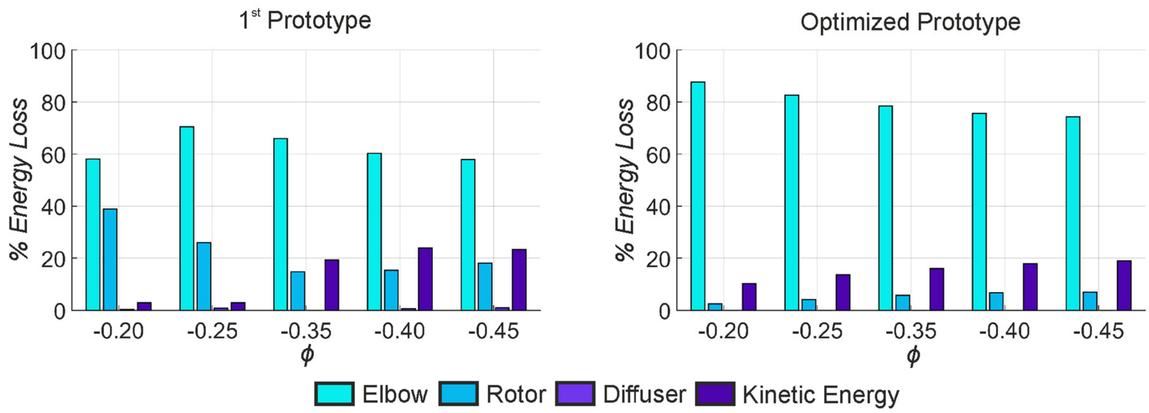

Figure 19. Comparison of the loss distribution in reverse mode between the different elements of the first (left) and the optimized prototype (right).

4. CONCLUSIONS

In this paper, a CFD numerical model has been created and validated to analyse the flow patterns of two different OutFlow Radial turbines (first and optimized prototype), designed to be installed in a Twin Turbine Configuration of an Oscillating Water Column Wave energy devices.

The numerical model is characterized by the employment of radially-straight sidewalls for the periodic boundaries, which makes the construction of the model and the meshing operations much easier for non-experienced researchers. The comparison of the results with respect to previous experimental data has been really accurate for this new modelling strategy.

The results obtained from this numerical model have been also compared to a formerly published prototype to gain deeper knowledge of the performance of the turbine. Special attention has been paid to the reverse mode when the prototypes are working as a backflow preventer.

The study has demonstrated that the use of OutFlow Radial turbines within a Twin Turbines configuration is very interesting due to the complex structures created at the rotor inlet during the reverse mode. This produces an extremely good blockage of the flow that leads to an exceptional performance as an aerodynamic backflow preventer. It has been verified that modifying the blade geometry which resulted in a significant narrowing of the effective blade passage of the rotor is positive to improve its performance as backflow preventer. However, special care must be done during the optimization process in order to preserve the turbine efficiency in direct mode and do not penalize the overall suitability of this turbine for OWC devices.

Regarding the direct mode, it has been also verified that efficiencies above 75% can be reached without losing the blockage capacity in reverse mode. This is mainly achieved by the advantageous performance of the elbow, critical in reverse mode which resulted significantly dependant on the inner blade angle. Nevertheless, the results have shown that the kinetic energy in the diffuser continues to be the main source of loss in direct mode. Near future work will be focused on a new promising geometry to deal with this pending drawback.

It is finally concluded that the efficiency of the OutFlow Radial turbine could compete with axial turbines in the case of Twin Turbines Configuration. In any case, more research is required to compare, in a more global perspective, the suitability of these radial turbines with respect to axial architectures, considering manufacturing and operation costs and final energy production. In addition, it is necessary to open the scope and compare a Twin Turbines Configuration equipped with radial turbines with respect conventional bidirectional turbines, not only in terms of efficiency, but also in a wider perspective using a wave-to-wire model.

5. AUTHORS CONTRIBUTION

L.R.; build the numerical model, run the simulations, and extracted data from the model. B.P.: devised the project, analysed the data, and wrote the paper. M.G.: made the data postprocessing and created the figures. J.F.: helped with the figures and co-wrote the paper. F.C.: helped in the final details of the paper.

6. ACKNOWLEDGEMENTS

The authors acknowledge the support provided by "Centro Integrado de F.P. Mantenimiento y Servicios a la Producción de Langreo", with special mention to its Director when this work was carried out, Mr. F. Fanjul.
Additionally, the Spanish ‘‘Ministerio de Educación, Cultura y Deporte’’ and its "FPU Program" for the pre-doctoral research scholarship of Manuel García (Grant No. FPU15/04375) is gratefully acknowledged.

REFERENCES

[1] Parsons A, Gruet R. Ocean Energy: Key Trends and Statistics 2018. 2018.

[2] Directorate-General for Maritime Affairs and Fisheries. Market Study on Ocean Energy. Final report. 2018. https://doi.org/10.2771/89934.

[3] Falcão AFO, Henriques JCC. Oscillating-water-column wave energy converters and air turbines: A review. Renew Energy 2016;85:1391–424. https://doi.org/10.1016/j.renene.2015.07.086.

[4] Das TK, Halder P, Samad A. Optimal design of air turbines for oscillating water column wave energy systems: A review. Int J Ocean Clim Syst 2017;8:37–49. https://doi.org/10.1177/1759313117693639.

[5] Falcão AFO, Henriques JCC, Gato LMC. Self-rectifying air turbines for wave energy conversion: A comparative analysis. Renew Sustain Energy Rev 2018;91:1231–41. https://doi.org/10.1016/j.rser.2018.04.019.

[6] Jayashankar V, Anand S, Geetha T, Santhakumar S, Jagadeesh Kumar V, Ravindran M, et al. A twin unidirectional impulse turbine topology for OWC based wave energy plants. Renew Energy 2009;34:692–8. https://doi.org/10.1016/j.renene.2008.05.028.

[7] Takao M, Setoguchi T, Kaneko K, Kim TH, Maeda H, Inoue M. Impulse Turbine for Wave Power Conversion with Air Flow Rectification System. Internatinal J Offshore Polar Eng 2002;12:142–6.

[8] Mala K, Jayaraj J, Jayashankar V, Muruganandam TM, Santhakumar S, Ravindran M, et al. A twin unidirectional impulse turbine topology for OWC based wave energy plants - Experimental validation and scaling. Renew Energy 2011;36:307–14. https://doi.org/10.1016/j.renene.2010.06.043.

[9] Takao M, Takami A, Okuhara S, Setoguchi T. A twin unidirectional impulse turbine for wave energy conversion. J Therm Sci 2011;20:394–7. https://doi.org/10.1007/s11630-011-0486-1.

[10] Takao M, Setoguchi T. Air Turbines for Wave Energy Conversion. Int J Rotating Mach 2012;2012:1–10. https://doi.org/10.1155/2012/717398.

[11] Pereiras B, Valdez P, Castro F. Numerical analysis of a unidirectional axial turbine for twin turbine configuration. Appl Ocean Res 2014;47:1–8. https://doi.org/10.1016/j.apor.2014.03.003.

[12] Rodríguez L, Pereiras B, Fernández-Oro J, Castro F. Viability of unidirectional radial turbines for twin-turbine configuration of OWC wave energy converters. Ocean Eng 2018;154:288–97. https://doi.org/10.1016/j.oceaneng.2018.02.010.

[13] Rodríguez L, Pereiras B, Fernández-Oro J, Castro F. Optimization and experimental tests of a centrifugal turbine for an OWC device equipped with a twin turbines configuration. Energy 2019;171:710–20. https://doi.org/10.1016/j.energy.2019.01.029.

[14] Gato LMC, Henriques JCC, Ferreira DJ da CTN, Falcão AF d. O. Energy conversion system for use in bidirectional flows and its method of operation. WO 2018/056853 A1, 2018.

[15] Falcão AF de O, Gato LMC, Henriques JCC. Air turbine for applications in wave energy conversion. US 9976536 B2, 2018.

[16] Lopes BS, Gato LMC, Falcão AFO, Henriques JCC. Test results of a novel twin-rotor radial inflow self-rectifying air turbine for OWC wave energy converters. Energy 2019;170:869–79. https://doi.org/10.1016/j.energy.2018.12.078.

[17] Denniss T. Apparatus and method for extracting energy from a fluid. WO 2018/071963 A1, 2018.

[18] Fleming A, MacFarlane G, Hunter S, Denniss T. Power Performance Prediction for a Vented Oscillating Water Column Wave Energy Converter with a Unidirectional Air Turbine Power Take-off. Proc. Twelfth Eur. Wave Tidal Energy Conf., Cork, Ireland: 2017.

[19] Ansarifard N, Kianejad SS, Fleming A, Chai S. A radial inflow air turbine design for a vented oscillating water column. Energy 2019;166:380–91. https://doi.org/10.1016/j.energy.2018.10.068.

[20] Ansarifard N, Fleming A, Henderson A, Kianejad SS, Chai S, Orphin J. Comparison of inflow and outflow radial air turbines in vented and bidirectional OWC wave energy converters. Energy 2019;182:159–76. https://doi.org/10.1016/j.energy.2019.06.041.

[21] Otaola E, Garrido AJ, Lekube J, Garrido I. A Comparative Analysis of Self-Rectifying Turbines for the Mutriku Oscillating Water Column Energy Plant. Complexity 2019;2019:1–14. https://doi.org/10.1155/2019/6396904.

[22] Pereiras B, Castro F, Marjani A el, Rodríguez MA. An improved radial impulse turbine for OWC. Renew Energy 2011;36:1477–84. https://doi.org/10.1016/j.renene.2010.10.013.

[23] Inoue M, Kaneko K, Setoguchi T, Shimamoto K. Studies on Wells Turbine for Wave Power Generator : 4th Report, Starting and Running Characteristics in Periodically Oscillating Flow. Bull JSME 1986;29:1177–82. https://doi.org/10.1299/jsme1958.29.1177.

[24] Dixon SL, Hall CA. Fluid mechanics and thermodynamics of turbomachinery. 5th ed. Oxford: Elsevier Butterworth–Heinemann; 2005.

[25] Persico G, Pini M, Dossena V, Gaetani P. Aerodynamic Design and Analysis of Centrifugal Turbine Cascades. Vol. 6C Turbomach., ASME; 2013, p. V06CT40A019. https://doi.org/10.1115/GT2013-95770.

[26] Pini M, Persico G, Casati E, Dossena V. Preliminary Design of a Centrifugal Turbine for Organic Rankine Cycle Applications. J Eng Gas Turbines Power 2013;135:042312. https://doi.org/10.1115/1.4023122.